Exact duality and dual Monte Carlo simulation for the bosonic Hubbard model

F. Hébert, G. G. Batrouni, and H. Mabilat
Institut Non-Linéaire de Nice, Université de Nice–Sophia Antipolis, 1361 route des Lucioles, 06560 Valbonne, France
(Received 3 November 1999)

We derive the exact dual to the bosonic Hubbard model. The dual variables take the form of conserved current loops (local and global). Previously this has been done only for the very soft core model at very high density. No such approximations are made here. In particular, the dual of the hard core model is shown to have a very simple form, which is then used to construct an efficient Monte Carlo algorithm which is quite similar to the World Line algorithm but with some important differences. For example, with this algorithm we can measure easily the correlation function of the order parameter (Green function), a quantity which is extremely difficult to measure with the standard World Line algorithm. We demonstrate the algorithm for the one and two dimensional hardcore bosonic Hubbard models. We present results especially for the Green function and zero-mode filling fraction in the two dimensional hardcore model.

I. INTRODUCTION

Since its discovery by Kramers and Wannier,[1] duality has continued to play an important role in physics. Originally, duality related the ''high-temperature'' phase of one system to the ''low-temperature'' phase of another. But it has long been realized that duality is more general than what is encountered in thermal statistical physics. In the case of quantum phase transitions, for example, high and low temperatures are replaced by high- and low-coupling constants that determine the size of quantum fluctuations. As an example in the thermal case, the two-dimensional Ising model is self dual, i.e., its low temperature phase is mapped onto the high-temperature phase of its dual, which is also an Ising model. This allowed Kramers and Wannier[1] to determine its exact critical temperature. The nature of the dual and the question of self-duality depend on several factors like the symmetry group of the action, the type of model (spin, gauge, etc), and the dimensionality.[2] Duality has found many applications.[2,3] For example, a very interesting recent application was to show that the bosonization of fermionic systems in any number of dimensions can be effected using the duality transformation.[4]

In quantum systems, such as the bosonic Hubbard model, an *approximate* duality transformation has been used to express the partition function in terms of conserved electric current loops.[5] This transformation is approximate in two ways: (1) The boson density is assumed to be very high, in other words the model is necessarily very soft core, and (2) the Villain form of the action[6] is assumed. Because of this, the dual model thus obtained is not even the dual of the Hubbard model but that of the quantum phase model (QPM). Still, this formulation was used very productively to study various aspects of the ground state phase diagram of the QPM numerically[5,7] and analytically.[8,9] However, to study the bosonic Hubbard model with no approximations (other than Trotter discretization), one still had to use one of the other available algorithms. The World Line algorithm[10] proved very useful in one and two dimensions with or without disorder.[11,12] Improvements on this (in the hard core case) came in the form of the loop (or cluster) algorithm[13] and the continuous time cluster algorithm.[14] These two algorithms were designed to eliminate long relaxation times (critical slowing down) at half filling and in the absence of longer-range interactions (like next near neighbor). When these conditions are not met these algorithms become extremely inefficient. In addition to questions of inefficiency, a disadvantage shared by these algorithms is that even though one can calculate, rather easily, the superfluid density and other physical quantities such as the energy and compressibility[5,7,11–14] it is very difficult, if not impossible, to measure the correlation function of the order parameter (the Green function, G) which is a very interesting quantity. The ''worm'' algorithm[15] can be used to calculate G but seems to converge very slowly in two dimensions. The recently developed stochastic series expansion method[16] is very promising. It overcomes the inefficiencies of the loop algorithm, but whether it is efficient for measuring G is to be seen.

It is sometimes desirable to do the simulation in the canonical ensemble especially when studying questions of phase separation. To this end, we will first show here how to implement the duality transformation *exactly* following the method of Ref. 3. We will then construct a quantum Monte Carlo (QMC) algorithm valid in the canonical and grand canonical ensembles and with or without disorder. The efficiency of this algorithm does not deteriorate when the system is doped away from half filling or in the presence of longer range interactions. It also has the advantage of being able to calculate, rather easily, G in the grand canonical and canonical ensembles.

The paper is organized as follows. In Sec. II, we show the duality tranformation leaving the details for the appendix. In Sec. III, we simplify the results and construct the QMC algorithm for hardcore bosons. In Sec. IV, we discuss some algorithmic improvements and details and show tests of the algorithm in the one dimensional bosonic Hubbard model in the hardcore limit. In Sec. V, we present new simulation results for the two dimensional hardcore bosonic Hubbard model with near and next near neighbors. Section VI is for conclusions.

II. DUALITY TRANSFORMATION OF THE BOSONIC HUBBARD MODEL

A. The bosonic Hubbard model

We are interested in simulating models whose Hamiltonian has the form

$$H=-t\sum_{\langle rr'\rangle}(a_r^\dagger a_{r'}+a_{r'}^\dagger a_r)+V_0\sum_r\frac{\hat{n}_r(\hat{n}_r-1)}{2}+V_1\sum_{\langle rr'\rangle}\hat{n}_r\hat{n}_{r'}+V_2\sum_{\langle\langle rr'\rangle\rangle}\hat{n}_r\hat{n}_{r'}+\cdots-\mu\sum_r\hat{n}_r. \tag{1}$$

In this equation, t is the transfer integral (the hopping parameter) which sets the energy scale (in the simulations we set it equal to 1), μ is the chemical potential, V_0, V_1, and V_2 are, respectively, the contact, the near and the next near neighbor interactions. The dots stand for other longer range interactions that can be added. On the square lattice, the next near neighbor is chosen along the diagonal, while in one dimension the choice is the obvious one. a_r and $a_r^\dagger$ are destruction and creation operators on site r satisfying the usual softcore boson commutation laws, $[a_r,a_{r'}^\dagger]=\delta_{r,r'}$, and $\hat{n}_r=a_r^\dagger a_r$ is the number operator on site r. $\langle rr'\rangle$ and $\langle\langle rr'\rangle\rangle$ label sums over near and next near neighbors. The first term which describes the hopping of the bosons among near neighbor sites gives the kinetic energy.

The quantum statistical mechanics of this system is given by the partition function Z,

$$Z=\mathrm{Tr}\,(e^{-\beta H}),\qquad =\sum_{\{\psi\}}\langle\psi|e^{-\beta H}|\psi\rangle, \tag{2}$$

where β is the inverse temperature and the sum runs over a complete set of states. The expectation value of a quantum operator is given by

$$\langle\mathcal{O}\rangle=\frac{1}{Z}\mathrm{Tr}(\mathcal{O}e^{-\beta H}). \tag{3}$$

B. Path integral representation

We now need to find a c-number representation of the partition function, which can then be incorporated into a simulation algorithm. There are several such representations.

The occupation number representation is defined by the eigenstates $|\mathbf{n}\rangle$ of the number operator $a_r^\dagger a_r$,

$$|\mathbf{n}\rangle=\left[\prod_r\frac{(a_r^\dagger)^{n_r}}{\sqrt{n_r!}}\right]|0\rangle, \tag{4}$$

where $|\mathbf{n}\rangle$ stands for a complete set of n_r, $|\mathbf{n}\rangle=|n_1,n_2,\cdots\rangle$ where n_r is the number of bosons at site r. In this representation the resolution of unity reads

$$\mathbf{1}=\sum_{\mathbf{n}}|\mathbf{n}\rangle\langle\mathbf{n}|. \tag{5}$$

Another common representation uses coherent states $|\Phi\rangle$, i.e., eigenstates of the destruction operator,

$$a_r|\Phi\rangle=\phi_r|\Phi\rangle,\qquad \langle\Phi|a_r^\dagger=\langle\Phi|\phi_r^\star, \tag{6}$$

where the eigenvalues ϕ_r are complex numbers defined on the sites of the lattice. We completely define this state with the vector $\Phi=(\phi_1,\ldots,\phi_r,\ldots)$.

In terms of the occupation number representation vacuum $|0\rangle$ the coherent state $|\Phi\rangle$ is defined as

$$|\Phi\rangle=\exp\left(\sum_r\phi_r a_r^\dagger\right)|0\rangle, \tag{7}$$

so that its projection on an occupation number state is

$$\langle\mathbf{n}|\Phi\rangle=\prod_r\left(\frac{\phi_r^{n_r}}{\sqrt{n_r!}}\right). \tag{8}$$

With this normalization we obtain the inner product of two coherent states

$$\langle\Psi|\Phi\rangle=\exp\left(\sum_r\psi_r^\star\phi_r\right), \tag{9}$$

and the resolution of unity

$$\mathbf{1}=\int\prod_r\frac{d^2\phi_r}{\pi}\exp\left(-\sum_r|\phi_r|^2\right)|\Phi\rangle\langle\Phi|. \tag{10}$$

The interaction and chemical potential part of the Hamiltonian are more easily expressed in the occupation number representation while a coherent state representation is well suited to the treatment of the kinetic term. We will use both successively. We write the partition function, Eq. (2), as

$$Z=\sum_{\{\mathbf{n}\}}\langle\mathbf{n}|e^{-\beta H}|\mathbf{n}\rangle=\sum_{\{\mathbf{n}\}}\langle\mathbf{n}|e^{-\delta H}e^{-\delta H}\cdots e^{-\delta H}|\mathbf{n}\rangle, \tag{11}$$

where $\delta\equiv\beta/L_\tau$, and L_τ is a large enough integer such that $\delta\ll 1$. We express the partition function this way because we can now express the exponentials in Eq. (11) in a form suitable for easy evaluation. Between each pair of exponentials we introduce the resolution of unity, Eq. (5). We find

$$Z=\sum_{\{\mathbf{n}_\tau\}}\langle\mathbf{n}_1|e^{-\delta H}|\mathbf{n}_{L_\tau}\rangle\langle\mathbf{n}_{L_\tau}|e^{-\delta H}|\mathbf{n}_{L_\tau-1}\rangle\cdots\times\cdots\langle\mathbf{n}_3|e^{-\delta H}|\mathbf{n}_2\rangle\langle\mathbf{n}_2|e^{-\delta H}|\mathbf{n}_1\rangle. \tag{12}$$

As δ is small,

$$e^{-\delta H}=e^{-\delta(T+V)}\approx e^{-\delta V/2}e^{-\delta T}e^{-\delta V/2}+\mathcal{O}(\delta^3), \tag{13}$$

where T is the kinetic energy and V contains the interaction and chemical potential terms.

The partition function now becomes

$$Z=\sum_{\{\mathbf{n}_\tau\}}\langle\mathbf{n}_1|e^{-\delta V/2}e^{-\delta T}e^{-\delta V/2}|\mathbf{n}_{L_\tau}\rangle\cdots \times\cdots\langle\mathbf{n}_2|e^{-\delta V/2}e^{-\delta T}e^{-\delta V/2}|\mathbf{n}_1\rangle =\sum_{\{\mathbf{n}_\tau\}}\prod_\tau[e^{-\delta V(\mathbf{n}_\tau)}] \langle\mathbf{n}_1|e^{-\delta T}|\mathbf{n}_{L_\tau}\rangle\cdots\langle\mathbf{n}_2|e^{-\delta T}|\mathbf{n}_1\rangle. \quad (14)$$

The error introduced by neglecting commutators of T and V is of order $L_\tau\delta^3=\beta\tau^2$ for the partition function.

We now introduce unity operators expressed in terms of coherent states [Eq. (10)] around the kinetic terms

$$Z=\sum_{\{\mathbf{n}_\tau\}}\int\prod_{r,\tau}\left(\frac{d^2\phi_{r,\tau}d^2\tilde{\phi}_{r,\tau}}{\pi^2}e^{-(|\phi_{r,\tau}|^2+|\tilde{\phi}_{r,\tau}|^2)}\right) \times\prod_\tau[e^{-\delta V(\mathbf{n}_\tau)}]\langle\mathbf{n}_1|\tilde{\Phi}_1\rangle\langle\tilde{\Phi}_1|e^{-\delta T}|\Phi_{L_\tau}\rangle\langle\Phi_{L_\tau}|\mathbf{n}_{L_\tau}\rangle \times\langle\mathbf{n}_{L_\tau}|\tilde{\Phi}_{L_\tau}\rangle\langle\tilde{\Phi}_{L_\tau}|e^{-\delta T}|\Phi_{L_\tau-1}\rangle\langle\Phi_{L_\tau-1}|\mathbf{n}_{L_\tau-1}\rangle\cdots \times\langle\mathbf{n}_2|\tilde{\Phi}_2\rangle\langle\tilde{\Phi}_2|e^{-\delta T}|\Phi_1\rangle\langle\Phi_1|\mathbf{n}_1\rangle. \quad (15)$$

Notice that we need to introduce two sets of L_τ coherent states, the Φ and $\tilde{\Phi}$. We can avoid introducing two different representations (occupation and coherent) and only use coherent states. But then, we would have to decouple the interaction terms in order to integrate them out. At the end this would lead to the same results, but it would be more difficult to recover a simple expression for Z.

At this stage, it is customary to neglect terms of order 2 and higher in δ in the expectation value of $\exp(-\delta T)$ since their contribution goes to zero with δ. While this is correct and would still allow us to calculate thermodynamic quantities such as $\langle E\rangle$, it would not be sufficient to calculate the Green function, $G(|r-r'|)=\langle a_r a^\dagger_{r'}\rangle$, at distances $|r-r'|>1$ (see below).

For this reason, it is very important to keep higher orders. We start by keeping all such higher order terms of $\exp(-\delta T)$. Since T is quadratic

$$T=\sum_{rr'}a^\dagger_r K^{rr'}a_{r'}=\mathbf{a}^\dagger\mathbf{K}\mathbf{a}, \quad (16)$$

where $\mathbf{K}$ is a c-number matrix, we can use the following identity[17]

$$\langle\Psi|e^{-\delta\mathbf{a}^\dagger\mathbf{K}\mathbf{a}}|\Phi\rangle=\langle\Psi|:\exp(-\mathbf{a}^\dagger[1-e^{-\delta\mathbf{K}}]\mathbf{a}):|\Phi\rangle, \quad (17)$$

where $:\mathcal{O}:$ indicates that the operator $\mathcal{O}$ is normal ordered. Equation (17) may now be expressed as[17]

$$\langle\Psi|e^{-\delta\mathbf{a}^\dagger\mathbf{K}\mathbf{a}}|\Phi\rangle=\langle\Psi|\Phi\rangle\exp(-\Psi^\dagger[1-e^{-\delta\mathbf{K}}]\Phi), =e^{\Psi^\dagger\Phi}\exp(-\Psi^\dagger[1-e^{-\delta\mathbf{K}}]\Phi). \quad (18)$$

Expanding the exponential term in Eq. (18), one finds

$$e^{\Psi^\dagger\Phi}\exp-\left(\Psi^\dagger\left[\delta\mathbf{K}-\frac{\delta^2\mathbf{K}^2}{2!}+\frac{\delta^3\mathbf{K}^3}{3!}-\frac{\delta^4\mathbf{K}^4}{4!}+\cdots\right]\Phi\right). \quad (19)$$

For simplicity, we will illustrate how to proceed by using a one dimensional L_x-site lattice with periodic boundary conditions. All nearest neighbors $\langle rr'\rangle$ pairs are labeled by choosing $r'=r+1$ and summing over all r. The same can be easily done in any dimensionality. We write $\mathbf{K}$ as $\mathbf{K}=-t\mathbf{K}_1$ where $\mathbf{K}_1$ is the matrix that connects nearest neighbors: If r and r' are nearest neighbors then $K_1^{rr'}=1$, otherwise $K_1^{rr'}=0$. It is easy to show that

$$\mathbf{K}^2=(-t)^2(2\mathbf{I}+\mathbf{K}_2),$$
$$\mathbf{K}^3=(-t)^3(3\mathbf{K}_1+\mathbf{K}_3),$$
$$\mathbf{K}^4=(-t)^4(6\mathbf{I}+4\mathbf{K}_2+\mathbf{K}_4)\cdots, \quad (20)$$

where $\mathbf{K}_L$ generates hops of L lattice spacings.

Introducing this into Eq. (19) and keeping only the leading order term in δ for each matrix, $\mathbf{K}_L$, we get

$$\exp\left\{\Psi^\dagger\left[\mathbf{I}+(\delta t)\mathbf{K}_1+\frac{(\delta t)^2\mathbf{K}_2}{2!}+\frac{(\delta t)^3\mathbf{K}_3}{3!}+\frac{(\delta t)^4\mathbf{K}_4}{4!}+\cdots\right]\Phi\right\}. \quad (21)$$

Substituting the preceding expression into Eq. (15), using Eq. (8) to express the scalar products, and neglecting higher order terms, we get the following expression for the partition function:

$$Z=\sum_{\{\mathbf{n}_\tau\}}\int\prod_{r,\tau}\left(\frac{d^2\phi_{r,\tau}d^2\tilde{\phi}_{r,\tau}}{\pi^2}\right)\mathcal{P}(\Phi,\tilde{\Phi},\mathbf{n}), \quad (22)$$

where the weight $\mathcal{P}$ is given by

$$\mathcal{P}(\Phi,\tilde{\Phi},\mathbf{n})=\prod_\tau[e^{-\delta V(\mathbf{n}_\tau)}]\prod_{r,\tau}\left[e^{-(|\phi_{r,\tau}|^2+|\tilde{\phi}_{r,\tau}|^2)} \times\frac{(\tilde{\phi}_{r,\tau}\phi^\star_{r,\tau})^{n_{r,\tau}}}{n_{r,\tau}!}e^{\tilde{\phi}^\star_{r,\tau+1}\phi_{r,\tau}}\right] \times\exp\left\{\sum_{r,r',\tau}\left(\tilde{\phi}^\star_{r',\tau+1}\left[\delta t K_1^{r'r}+\frac{(\delta t)^2K_2^{r'r}}{2!}+\cdots\right]\phi_{r,\tau}\right)\right\}. \quad (23)$$

We reiterate that as $\delta t\to 0$, the contributions of multiple hops, i.e., $\mathbf{K}_L$ where $L>1$, to the energy and other local physical quantities vanish since they are of higher order in δt. However, this is not true for nonlocal quantities such as $G(r)=\langle a_0 a^\dagger_r\rangle$ for $r>1$. Keeping the higher order terms will give us the generating functional for this correlation function. Notice, however, that we have kept only the terms nec-

essary to calculate each quantity to leading order in δ. Therefore the algorithm will have systematic Trotter errors of order $\beta\delta$.

C. Dual formulation

In order to perform the integration over the original variables and obtain the dual formulation of Z, we express the $\phi_{r,\tau}$ and $\tilde{\phi}_{r,\tau}$ as,

$$\phi_{r,\tau}=\rho_{r,\tau}\exp(i\theta_{r,\tau}), \tag{24}$$

which gives the following expression for Z

$$\begin{aligned}Z=\int \mathcal{D}\Psi\prod_{r,\tau}\Bigg\{&\frac{1}{n_{r,\tau}!}(\tilde{\rho}_{r,\tau}\rho_{r,\tau})^{n_{r,\tau}}e^{i(\tilde{\theta}_{r,\tau}-\theta_{r,\tau})n_{r,\tau}}\\&\times\exp(\tilde{\rho}_{r,\tau+1}\rho_{r,\tau}e^{-i(\tilde{\theta}_{r,\tau+1}-\theta_{r,\tau})})\\&\times\exp(\delta t\tilde{\rho}_{r+1,\tau+1}\rho_{r,\tau}e^{-i(\tilde{\theta}_{r+1,\tau+1}-\theta_{r,\tau})})\\&\times\exp(\delta t\tilde{\rho}_{r,\tau+1}\rho_{r+1,\tau}e^{-i(\tilde{\theta}_{r,\tau+1}-\theta_{r+1,\tau})})\\&\times\exp\left(\frac{(\delta t_{r,\tau})^2}{2!}\tilde{\rho}_{r+2,\tau+1}\rho_{r,\tau}e^{-i(\tilde{\theta}_{r+2,\tau+1}-\theta_{r,\tau})}\right)\\&\times\exp\left(\frac{(\delta t_{r,\tau})^2}{2!}\tilde{\rho}_{r,\tau+1}\rho_{r+2,\tau}e^{-i(\tilde{\theta}_{r,\tau+1}-\theta_{r+2,\tau})}\right)\cdots\Bigg\}.\end{aligned} \tag{25}$$

Dots stand for all longer range hopping terms and $\int\mathcal{D}\Psi$ stands for

$$\begin{aligned}\int\mathcal{D}\Psi=\sum_{\{n_{r,\tau}\}}\int\prod_{r,\tau}\Bigg[&\rho_{r,\tau}d\rho_{r,\tau}\tilde{\rho}_{r,\tau}d\tilde{\rho}_{r,\tau}\frac{d\theta_{r,\tau}}{\pi}\frac{d\tilde{\theta}_{r,\tau}}{\pi}\\&\times e^{-(|\rho_{r,\tau}|^2+|\tilde{\rho}_{r,\tau}|^2)}\Bigg]e^{-\Sigma_\tau\delta V(\mathbf{n}_\tau)}.\end{aligned} \tag{26}$$

As expected, only gauge invariant phase differences appear in Eq. (25). Therefore, instead of performing the integrals over the gauge dependent site phases, $\theta_{r,\tau}$ and $\tilde{\theta}_{r,\tau}$, we express the partition function in terms of the following gauge invariant quantities

$$\begin{aligned}\Theta^0_{r,\tau}&=\theta_{r,\tau}-\tilde{\theta}_{r,\tau},\\\Theta^1_{r,\tau}&=\theta_{r+1,\tau}-\theta_{r,\tau},\\\tilde{\Theta}^0_{r,\tau}&=\tilde{\theta}_{r,\tau+1}-\theta_{r,\tau},\\\tilde{\Theta}^1_{r,\tau}&=\tilde{\theta}_{r+1,\tau}-\tilde{\theta}_{r,\tau}.\end{aligned} \tag{27}$$

We use indices 0 and 1 to label the imaginary-time and $\hat{x}$ directions. In higher dimension, we would have 2 corresponding to the $\hat{y}$ direction, 3 to $\hat{z}$ . . . .

This variable change results in a nontrivial Jacobian, which was derived in Ref. 3. It was shown[3] that this Jacobian is only the product of two kinds of constraints on the gauge variables and that it can be written as

$$\begin{aligned}\mathcal{J}=\sum_{\{N^\mu_{r,\tau}\}}\sum_{\{J^\mu_{r,\tau}\}}{}'\prod_{r,\tau}[&e^{i\Theta^0_{r,\tau}(J^0_{r,\tau-1}+N^0_r)}\\&\times e^{i\tilde{\Theta}^0_{r,\tau}(J^0_{r,\tau}+N^0_r)}e^{i\Theta^1_{r,\tau}(J^1_{r,\tau}+N^1_\tau)}],\end{aligned} \tag{28}$$

where the integer valued variables, $N^\mu_{r,\tau}$ and $J^\mu_{r,\tau}$, represent conserved currents and are, in fact, the dual variables.[3] The origin of these constraints is that the sum of the bond variables along any directed closed path must be zero as is seen from their definition in Eq. (27). $\tilde{\Theta}^1$ does not appear in the Hamiltonian and so has been eliminated in the Jacobian. For a detailed discussion of these constraints and their relation to duality, the strong coupling expansion etc., see Ref. 3.

The global currents, $N^\mu_{r,\tau}$, traverse the system from one end to the other and are required by the periodic boundary conditions. N^0_r is a global current in the time direction and, therefore, does not depend on the coordinate τ. Similarly, N^1_τ, the global current in the $\hat{x}$ direction depends only on τ (in two dimensions it would also depend on y). The local currents, $J^\mu_{r,\tau}$, form topologically trivial closed loops, i.e., they do not wrap around the system from one end to the other. The sum of the $J^\mu_{r,\tau}$ configurations is restricted to be only over conserved current configurations: The total current entering a site equals the current leaving. This is indicated by the prime on the sum. We will see below that this current has a simple physical interpretation.

With this variable change and Jacobian, Z becomes

$$\begin{aligned}Z=\int \mathcal{D}\Psi\prod_{r,\tau}\Bigg\{&\frac{1}{n_{r,\tau}!}(\tilde{\rho}_{r,\tau}\rho_{r,\tau})^{n_{r,\tau}}e^{-i\Theta^0_{r,\tau}n_{r,\tau}}\\&\times\exp(\tilde{\rho}_{r,\tau+1}\rho_{r,\tau}e^{-i\tilde{\Theta}^0_{r,\tau}})\\&\times\exp(\delta t\tilde{\rho}_{r+1,\tau+1}\rho_{r,\tau}e^{-i(\tilde{\Theta}^0_{r+1,\tau}+\Theta^1_{r,\tau})})\\&\times\exp(\delta t\tilde{\rho}_{r,\tau+1}\rho_{r+1,\tau}e^{-i(\tilde{\Theta}^0_{r,\tau}-\Theta^1_{r,\tau})})\\&\times\exp\left[\frac{(\delta t_{r,\tau})^2}{2!}\tilde{\rho}_{r+2,\tau+1}\rho_{r,\tau}e^{-i(\tilde{\Theta}^0_{r+2,\tau}+\Theta^1_{r+1,\tau}+\Theta^1_{r,\tau})}\right]\\&\times\exp\left[\frac{(\delta t_{r,\tau})^2}{2!}\tilde{\rho}_{r,\tau+1}\rho_{r+2,\tau}e^{-i(\tilde{\Theta}^0_{r,\tau}-\Theta^1_{r,\tau}-\Theta^1_{r+1,\tau})}\right]\cdots\\&\times e^{i\Theta^0_{r,\tau}(J^0_{r,\tau-1}+N^0_r)}e^{i\tilde{\Theta}^0_{r,\tau}(J^0_{r,\tau}+N^0_r)}e^{i\Theta^1_{r,\tau}(J^1_{r,\tau}+N^1_\tau)}\Bigg\},\end{aligned} \tag{29}$$

where

$$\begin{aligned}\int\mathcal{D}\Psi=\sum_{\{N^\mu_{r,\tau}\}}\sum_{\{J^\mu_{r,\tau}\}}{}'\sum_{\{n_{r,\tau}\}}&\\\int\prod_{r,\tau}\Bigg[&\rho_{r,\tau}\frac{d\rho_{r,\tau}}{\pi}\tilde{\rho}_{r,\tau}\frac{d\tilde{\rho}_{r,\tau}}{\pi}d\Theta^0_{r,\tau}d\tilde{\Theta}^0{}_{r,\tau}d\Theta^1_{r,\tau}\\&\times e^{-(|\rho_{r,\tau}|^2+|\tilde{\rho}_{r,\tau}|^2)}\Bigg]e^{-\sum_\tau\delta V(\mathbf{n}_\tau)}.\end{aligned} \tag{30}$$

Integrating the original variables, Θ, ρ, and n leaves only the integer valued dual variables. The details are shown in the appendix. The result of this integration is a complicated

expression for the dual partition function involving several integer valued fields and constraints.

One can greatly simplify this expression by explicitly solving the constraints appearing in it (these constraints come from the integration of Θ), that is, by finding the allowed configurations of $N^{\mu}_{r,\tau}$ and $J^{\mu}_{r,\tau}$ and their associated Boltzmann weight. In the appendix we illustrate this for soft-core and hardcore bosons but concentrate on the hard core case where the dual partition function takes a particularly simple form.

III. QUANTUM MONTE CARLO ALGORITHM IN THE HARD CORE LIMIT

A. Partition function in the hardcore limit

As shown in the Appendix, we can express the partition function and other physical quantities in terms of only one field, the total conserved hard-core current $N^{\mu}_{r,\tau}+J^{\mu}_{r,\tau}$. By hard-core, we mean that the total current, $N^{\mu}_{r,\tau}+J^{\mu}_{r,\tau}$, traversing a bond in the imaginary time direction takes the values 0 or 1, while in a spatial direction it takes the values $0,\pm 1$. We have also chosen, without any loss of generality, to keep $\Sigma_{r,\tau}J^{\mu}_{r,\tau}=0$. Notice that the total time currents are never negative: The bosons cannot go backward in the imaginary time direction.

The partition function in the grand canonical case reads

$$Z=\sum_{\{J,N\}}\mathcal{P}(N,J),$$
$$=\sum_{\{J,N\}}\left\{\prod_{L}\left[\left(\frac{(\delta t)^{L}}{L!}\right)^{N_L}\right]\times e^{\delta\mu\sum_{r,\tau}N^{0}_{r}}e^{-\delta V N_{V_1}}e^{-\delta V N_{V_2}}\right\}, \tag{31}$$

where N_L is the number of jumps of length L on the lattice, N_{V_1} the number of near neighbor time currents, and N_{V_2} the number of next-near-neighbor time currents.

The chemical potential appears in an exponential of $\beta\Sigma_{r,\tau}N^{0}_{r,\tau}$. So the number of particles in the system is simply

$$\langle\hat{n}\rangle=\frac{1}{\beta}\frac{\partial}{\partial\mu}\ln Z=\left\langle\frac{1}{L_\tau}\sum_{r,\tau}N^{0}_{r}\right\rangle=\left\langle\sum_{r}N^{0}_{r}\right\rangle, \tag{32}$$

which demonstrates that the current simply represents the current of bosons crossing the lattice in the positive imaginary time direction. So we have current lines crossing the lattice and the sampling of the configurations is achieved by deforming these lines. If one wants to work in the canonical ensemble, one simply has to fix the number of current lines.

The effect of interactions is simply given by multiplying the weight by $e^{-\delta V_1}$ ($e^{-\delta V_2}$) for every pair of near-neighbor (next-near-neighbor) time currents.

The term containing t, coming from the expansion of the hopping term, also has a simple physical interpretation: Kinetic energy arises when there are jumps, i.e., spatial currents. This term can also be written as

$$\prod_{L}\left[\left(\frac{1}{L!}\right)^{N_L}\right](\delta t)^{N_H}. \tag{33}$$

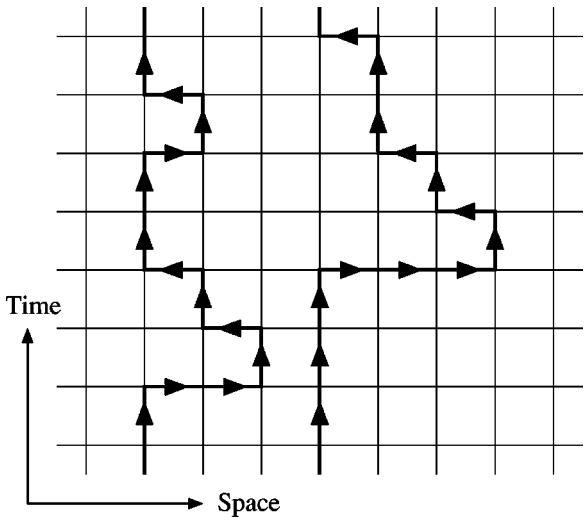

FIG. 1. Example of a configuration of the conserved boson current on a 1D lattice.

The exponent N_H of δt is the number of nonzero spatial currents $N_H=\Sigma_L N_L=\Sigma_{r,\tau}|N^{1}_{\tau}+J^{1}_{r,\tau}|$ but there is a combinatorial prefactor arising from multiple jumps.

We therefore have a simple physically intuitive expression for Z which allows easy evaluation of the Boltzmann weight. For example in Fig. 1, there are 7 single jumps, one double jump, and one triple jump. There are also one pair of near neighbor time slices and one pair of next near neighbor. So the weight associated with this configuration is

$$\frac{(\delta t)^{12}}{2!3!}e^{-\delta V_1}e^{-\delta V_2}. \tag{34}$$

B. Physical quantities

As shown above, we have for the particle number, $\hat{n}_{r,\tau}$,

$$\langle\hat{n}_{r,\tau}\rangle=\langle N^{0}_{r}+J^{0}_{r,\tau}\rangle. \tag{35}$$

Then the density-density correlation function reads

$$\langle n(r_1)n(r_2)\rangle=\frac{1}{L_\tau}\left\langle\sum_{\tau}(N^{0}_{r_1}+J^{0}_{r_1,\tau})(N^{0}_{r_2}+J^{0}_{r_2,\tau})\right\rangle, \tag{36}$$

and the structure factor, $S(\vec{k})$, is its Fourier transform.

We now focus on the canonical case. The energy is given by $\langle E\rangle=-\partial/\partial\beta\ln Z$ and therefore by

$$\langle E\rangle=\frac{1}{\beta}\langle\delta V_1 N_{V_1}+\delta V_2 N_{V_2}-N_H\rangle. \tag{37}$$

The meaning of the three terms is transparent. The first two are the near and next near neighbor potential energies, and the last, which comes from the jumps, is the kinetic energy.

The superfluid density is related to the winding number, W, by[11,12]

$$\rho_s=\frac{\langle W^2\rangle}{2t\beta}. \tag{38}$$

where W, given by $\Sigma_\tau N_\tau^1$, changes with the global spatial currents N_τ^1.

Finally, we are able to calculate easily the Green function, i.e., the correlation function of the order parameter,

$$G(L)=\frac{1}{2L_\tau L_x}\left\langle \sum_{r,\tau}\left(a_{r,\tau}a^\dagger_{r+L,\tau}+a_{r+L,\tau}a^\dagger_{r,\tau}\right)\right\rangle, \quad (39)$$

which, in isotropic cases, equals

$$G(L)=\frac{1}{L_\tau L_x}\langle a_{r,\tau}a^\dagger_{r+L,\tau}\rangle. \quad (40)$$

This can be calculated directly from the generating functional, Eq. (31),

$$G(L)=\frac{1}{2L_\tau L_x}\frac{\partial}{\partial\left(\frac{\delta^L t^L}{L!}\right)}\ln Z, \quad (41)$$

which can be easily shown to equal

$$G(L)=\left\langle \frac{1}{2L_\tau L_x}\frac{L!}{(\delta t)^L}N_L\right\rangle. \quad (42)$$

We now see the importance of keeping multiple jump terms: The only configurations that contribute to $G(L)$ are those that contain jumps of length L. This is physically satisfying: There are correlations between two sites if they are directly connected by a jump. This quantity is also simple to calculate, we just need to count the number of multiple jumps on the lattice.

IV. ALGORITHMIC DETAILS

A. Evolution of the system

We begin by choosing an initial configuration of bosons. This is done by introducing a current line for each particle, i.e., by putting the corresponding global time currents to 1. Then the simulation proceeds by modifying these current lines using a Metropolis sampling scheme.

In one dimension, we can explore the whole phase space by simply applying two kinds of trial moves. First, we introduce local moves [Fig. 2(a)]: We visit sites sequentially and try to add a small (clockwise or anticlockwise) current loop. If this does not introduce currents greater than 1 or negative time currents, we accept or reject probalistically according to the Boltzmann weight, Eq. (31). In addition to these local moves, we have global ones [Fig. 2(b)] where we change the value of a spatial global current traversing the system. These moves change the winding number. The global moves have very low acceptance probability, which means that in practice, one cannot efficiently sample all the winding number sectors.

In order to do simulations in the grand canonical ensemble, one can introduce global moves along the time direction which will add or remove particles. One can also use the chemical potential term to introduce a disordered external potential by imposing a site dependent μ.

In two dimensions, we need to introduce two more types of trial moves to get topologically different configurations and ensure ergodicity. These moves are the one-particle twist and two-particle exchange shown in Fig. 3.

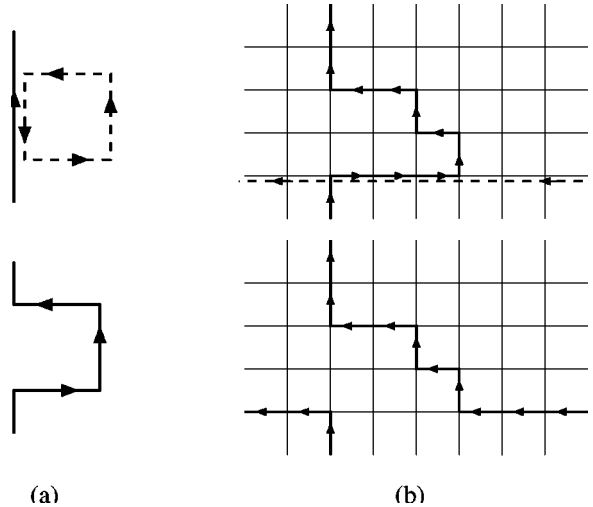

FIG. 2. The two kinds of trial moves for the one dimensional model: Local moves (a) and global moves (b).

B. Reweighting

As we have seen, multiple hopping terms are necessary for the calculation of the Green function, G. Consider the two configurations of Fig. 4, (a) contains only single jumps and has a weight $(\delta t)^4$, (b) contains one double jump and two single ones and so its weight is $(\delta t)^4/(2!)$. Both of them give a contribution of the same order in δ to Z. In the first case, since the position of each of the four jumps is arbitrary, the total number of such configurations grows as L_τ^4. Consequently, they give a finite contribution of order $L_\tau^4(\delta t)^4=(\beta t)^4$. For (b), only three jumps have arbitrary positions, which gives a final contribution of $L_\tau^3(\delta t)^4=(\beta t)^3\delta t$. Taking the $\delta\to 0$ limit, we see that the configurations with multiple jumps give no contribution to the partition function.

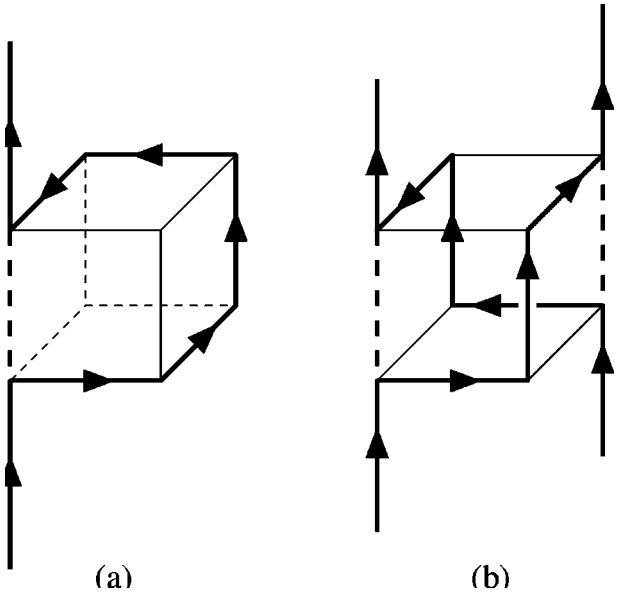

FIG. 3. Additional trial moves for the two dimensional case: One-particle twist (a) and two-particle exchange (b).

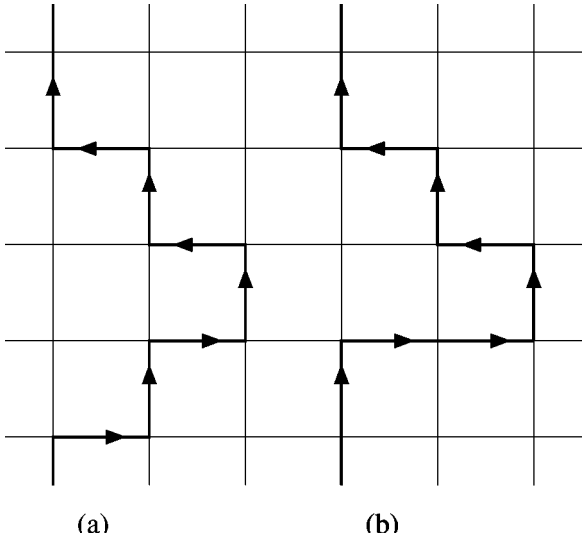

FIG. 4. A configuration of the conserved current for one boson (a) with four single jumps and (b) with one double jump and two single ones.

For the same reason, all configurations with jumps of size $L+1$ and many jumps of size L, do not give a finite contribution to $G(L)$. The only important configurations for $G(L)$ are those with one jump of size L ''combined with'' single jumps.

Sampling the configuration with the Boltzmann weight [Eq. (31)], the probability of having multiple jumps falls to zero as δ gets smaller. This causes a problem: We want small δ in order to reduce the Trotter discretization error which is proportional to δ. But in that limit the number of multiple jumps falls exponentially making it extremely difficult to calculate the Green function G.

To overcome this problem and calculate Green function efficiently, we introduce a reweighting scheme. We replace the weight $\mathcal{P}$ by a weight $\mathcal{P}_R$ designed to enhance configurations with multiple jumps.

Equations (31) and (42) show that a natural choice is to keep $\mathcal{P}_R=\mathcal{P}$ if there is no jump. When there are jumps we take

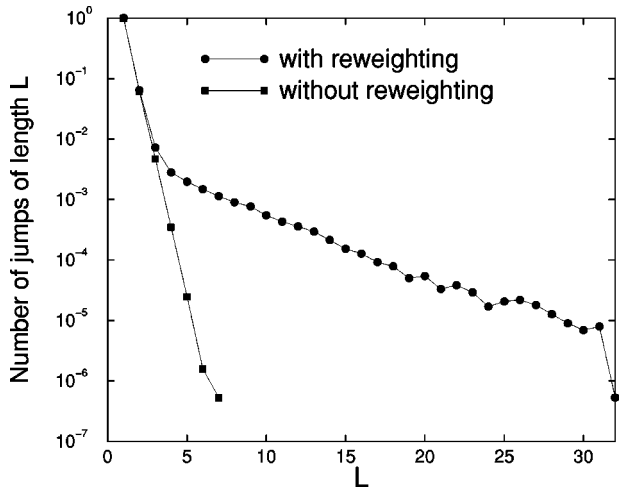

FIG. 5. Number of jumps of different lengths with and without reweighting for a system of 16 bosons on 32 sites at $\beta=4$.

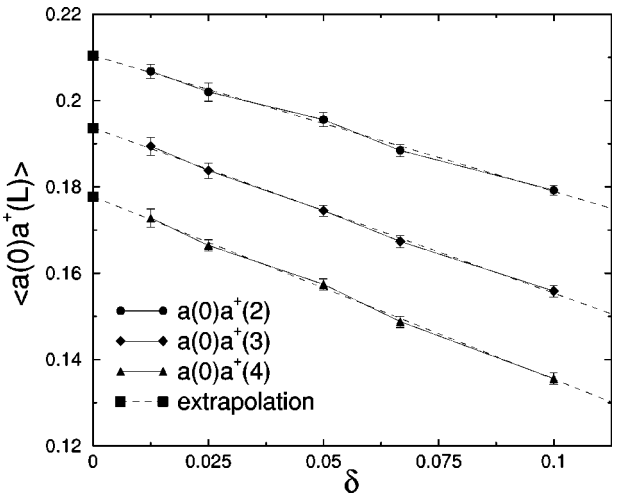

FIG. 6. Extrapolation to $\delta=0$ of the Green function at different distances for a system of 4 bosons on 8 sites at $\beta=4$ with only hardcore interactions.

$$\mathcal{P}_R=\frac{\mathcal{P}}{[(\delta t)^{\mathcal{M}-1}/\mathcal{M}!]}, \tag{43}$$

where $\mathcal{M}$ is the length of the biggest jump on the lattice. Since this changes the Boltzmann weight, we should compensate when measuring physical quantities. For the energy, we get (the sums run over all allowed configurations of the current)

$$\begin{aligned}\langle E\rangle&=\frac{1}{\beta}\frac{\sum(\delta V_1 N_{V_1}-N_H)\mathcal{P}}{\sum\mathcal{P}}\\&=\frac{1}{\beta}\frac{\sum(\delta V_1 N_{V_1}-N_H)\frac{\mathcal{P}}{\mathcal{P}_R}\mathcal{P}_R}{\sum\frac{\mathcal{P}}{\mathcal{P}_R}\mathcal{P}_R}\\&=\frac{1}{\beta}\frac{\sum(\delta V_1 N_{V_1}-N_H)[(\delta t)^{\mathcal{M}-1}/\mathcal{M}!]\mathcal{P}_R}{\sum[(\delta t)^{\mathcal{M}-1}/\mathcal{M}!]\mathcal{P}_R}\\&=\frac{1}{\beta}\frac{\langle(\delta V_1 N_{V_1}-N_H)[(\delta t)^{\mathcal{M}-1}/\mathcal{M}!]\rangle_{\mathcal{P}_R}}{\langle[(\delta t)^{\mathcal{M}-1}/\mathcal{M}!]\rangle_{\mathcal{P}_R}},\end{aligned} \tag{44}$$

and for the correlation function

$$G(L)=\frac{1}{2L_x\beta t}\frac{L!}{(\delta t)^{L-1}}\frac{\langle[(\delta t)^{\mathcal{M}-1}/\mathcal{M}!]N_L\rangle_{\mathcal{P}_R}}{\langle[(\delta t)^{\mathcal{M}-1}/\mathcal{M}!]\rangle_{\mathcal{P}_R}}. \tag{45}$$

This new reweighted algorithm increases dramatically the efficiency of the calculation of G. Figure 5 shows the number of jumps as a function of the length of the jump using the original and reweighted algorithms. As one can see, it falls

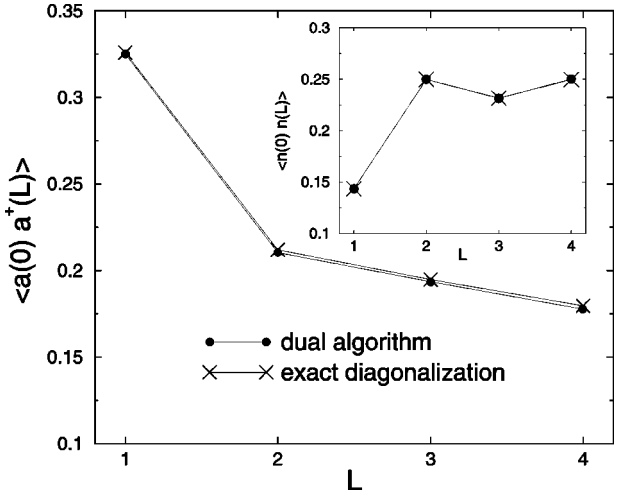

FIG. 7. Comparison of Green function and density-density correlation functions obtained with the dual algorithm and exact diagonalization techniques. The system contains 4 bosons on 8 sites with $\beta=4$ and only hardcore interactions.

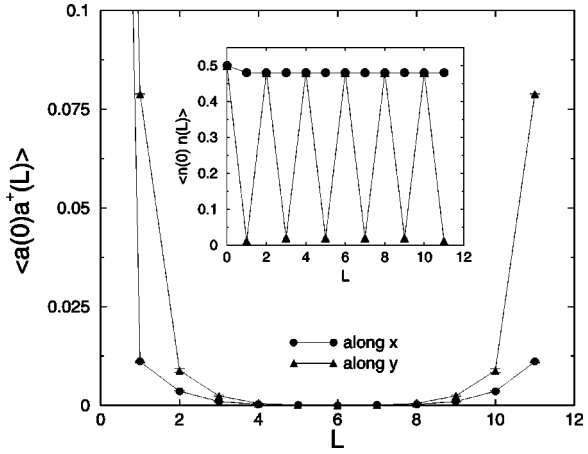

FIG. 8. Green function and density-density correlation function (inset) versus distance. 72 bosons on a 12×12 lattice with $V_1=0$, $V_2=3$, and $\beta=6$. The bosons form a striped incompressible solid.

exponentially with length in both cases. But, for the reweighted algorithm the slope is much weaker allowing frequent long jumps.

Reweighting favors long jumps which we can exploit to change the global spatial currents and thus the winding number. This algorithm then gives us exact results (after extrapolation to $\delta=0$) even for small size systems where the effect of nonzero W cannot be neglected.

That does not mean that using the Boltzmann weight without reweighting is of no interest. For big systems, nonzero winding numbers will have very small effect on local quantities and if one only wants these, there is no need for reweighting.

C. Tests of the algorithm

In order to test the algorithm, we compare its results with those of exact diagonalization on a small one-dimensional system (4 bosons on an 8 sites lattice at $\beta=4$ with only hard core interactions). We extrapolated our results to the $\delta=0$ limit before comparing (Fig. 6). The systematic errors are, as expected, clearly linear in δ. The extrapolated results are in excellent agreement (less than one percent error) with exact ones. Figure 7 shows comparison for density-density correlation function and G.

V. APPLICATIONS

As discussed above, with this algorithm (as with others before it) we can measure various physical quantities, such as the energy, the superfluid density, ρ_s, the density-density correlation function and its Fourier transform, the structure factor. What is new here is the ease with which we can measure the Green function, $\langle G(L)=a^\dagger(L)a(0)\rangle$ which, among other things, gives the number of condensed particles (occupation of the zero momentum mode). If one defines

$$G(0)=\frac{1}{L_\tau L_x}\sum_{r,\tau}\langle a_r^\dagger a_r\rangle, \tag{46}$$

then the Fourier transform of $G(L)$ equals the density of particles in the kth mode. In one dimension

$$\frac{1}{L_x}\sum_L e^{ikL}G(L)=N(k)=\frac{\langle a_k^\dagger a_k\rangle}{L_x}, \tag{47}$$

where

$$a_k^\dagger=\frac{1}{\sqrt{L_x}}\sum_r e^{-ikr}a_r^\dagger. \tag{48}$$

Using $G(L)$ and $N(0)$, one can easily obtain valuable information about the presence (or absence) of off-diagonal long range order (ODLRO), i.e., phase coherence at long distances.

We studied with this algorithm a two-dimensional 12×12 system of hardcore bosons at various fillings and interactions. We took $\beta=6$, which is a low enough temperature to access ground state properties. However, although the information is present in the configurations generated by this algorithm, we did not measure the Green-function off axis. We only measured it along the two lattice axes to reduce measurement time.

In Fig. 8 we show results for a 12×12 system at half filling and strong next-near-neighbor repulsion, $V_1=0$, $V_2=3$. The nnn repulsion makes the presence of next near neighbors too costly. Consequently, the bosons organize themselves into stripes with a $(\pi,0)$ [or $(0,\pi)$] ordering vector for the structure factor. In other words, the bosons form an incompressible gapped solid with stripes along the x or y axis. This is shown very clearly in the density-density correlation function shown in the inset of Fig. 8. Also shown in Fig. 8 is the Green function along the x and y axes. Notice that $G(L)=\langle a(0)a^\dagger(L)\rangle$ falls faster along the stripes (x axis) than in the transverse direction (y axis). This is because the energy cost for transverse hops, while high, is still finite. On the other hand, the cost for hops along the stripes is infinite because such hops would always lead to multiple occupancy of sites. In both cases, $G(L)$ goes to zero at long distance indicating the absence of superfluidity. This is confirmed with direct measurement of $\rho_s=\langle W^2\rangle/2t\beta$.

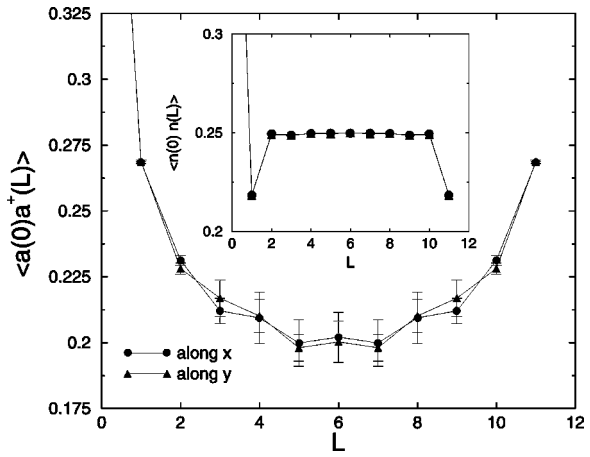

FIG. 9. Green function and density-density correlation function (inset) in the superfluid phase (72 bosons on a 12×12 lattice with $V_1=0$, $V_2=1$, and $\beta=6$). The system is isotropic and superfluid.

Reducing the nnn repulsion allows the long range order to melt and be replaced by ODLRO. This is shown in Fig. 9. The inset shows the density-density correlation functions along the x and y directions to be equal. The system is therefore spatially isotropic. This is confirmed by the isotropy (with error bars) of $G(L)$ along x and y. Also, notice that $G(L)$ is finite at long distance indicating symmetry breaking[18] (nonzero $\langle a\rangle$) and thus nonzero superfluid density which we also confirmed by direct measurement of $\rho_s=0.304\pm0.017$ from the winding number fluctuations.

If, instead of reducing V_2 at half filling, we now repeat the simulations that gave Fig. 8 but doped away from half filling, $\rho=0.472$, we observe more structure developing in the Green function. This is shown in Fig. 10. As before, the inset shows the density-density correlation function along x and y. As in Fig. 8, this shows clearly the presence of stripe order along the x axis. However we also see that $G(L)$ does not decay to zero at long distance. Instead, along the x axis, $G(L)$ resembles that in Fig. 9, i.e., tending towards a nonzero value at long distance indicating ODLRO and superfluidity. This is again confirmed by measuring directly the fluctuations of the winding number giving $\rho_s^x=0.027\pm0.003$. Along the y axis, $G(L)$ shows an oscillatory structure: At long distances, $G(L=\text{even})$ is greater than $G(L=\text{odd})$ and is almost equal to $G(L)$ along the x axis. This shows clearly that there is superfluidity along the y-axis, transverse to the direction of the stripes. Direct measurement gives $\rho_s^y=0.015\pm0.005$ which is less than ρ_s^x as may have been expected. The fact that both, long range density wave structure (diagonal order) and superfluidity (ODLRO) exist at the same time shows this phase to be a striped supersolid. This phase has been shown to have a finite critical velocity[12] and not to phase separate.[19] It is therefore stable. Doping above half filling will yield similar results: This model has particle-hole symmetry around $\rho=1/2$.

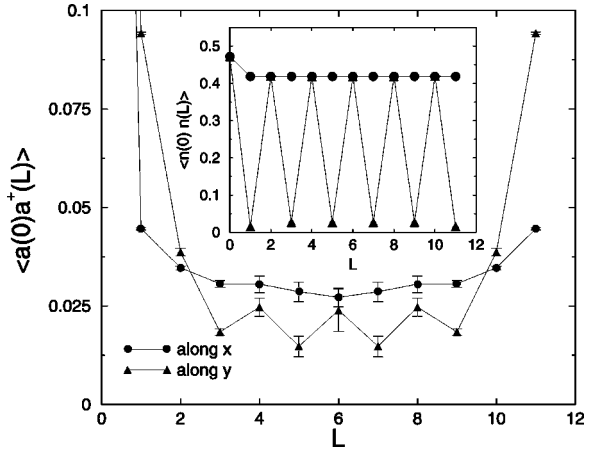

FIG. 10. Green function and density-density correlation function (inset) in the supersolid phase (68 bosons on a 12×12 lattice with $V_1=0$, $V_2=3$, and $\beta=6$). The system shows at the same time superfluidity and long range density modulations.

The wave structure in $G(L)$ along the y axis is easy to interpret physically. When the system was at half filling, the bosons could not hop along the stripes (since no double occupancy is allowed) and could only hop with difficulty transverse to the stripes into the empty sites due to the high-energy cost. When the system is doped below half filling, the bosons can easily hop *along* the stripes into neighboring holes. They still cannot easily hop an odd number of lattice spacings into the mostly empty stripes due to the high cost of nnn interactions. However, by hopping an even number of lattice spacings, they can fill in holes in the boson stripes, thus aquiring near neighbors at zero potential energy cost and avoiding next near neighbors which cost a lot of potential energy. This explains the smaller values of $G(L)$ for odd L along the y axis.

This also brings out an important point. The interpretation of a striped supersolid is *not* simply that the stripes form channels along which the bosons delocalize and the superfluid flows. While this does indeed happen, Fig. 10 shows clearly that there is also delocalization and superfluidity in the direction *transverse* to the stripes.

We now consider the case $V_1\neq0$, $V_2=0$. As is well established,[11,12,19] for $V_1>2$, $\rho=0.5$ the bosons are organized into an incompressible checkerboard solid, while for $V_1<2$ they delocalize into a superfluid. In other words, for large V_1, the Green function decays rapidly to zero as in Fig. 8 (but is isotropic in x and y), while for small V_1 it is nonzero for large separations signalling spontaneous symmetry breaking.

Measuring $G(L)$ as a function of V_1 enables us to calculate the filling fraction of the modes, $\langle a^\dagger(k_x,k_y)a(k_x,k_y)\rangle$ [Eq. (47)], as a function of interaction. Strictly speaking, this requires $G(|x-x'|,|y-y'|)$, i.e., off-axis as well as on-axis contributions to G. But, as explained above, we measured only on-axis contributions to G. We use this to obtain an estimate of the filling fraction as follows: Since we know that G is isotropic, and since we measured it along the lattice axis, we use these values to interpolate to lattice separations which we have not measured. For example, obtain $G(\sqrt{2})$, which corresponds to nnn, we interpolate the values of $G(1)$ and $G(2)$. The resulting Green function is Fourier transformed (two dimensional) to obtain the filling fraction. Figure 11(a) shows this filling fraction for the $k_x=0$ mode, $\rho_B(k_x=0)$, for different lattice sizes. We see a rapid transition around $V_1=2.1$ from a phase where the condensate fraction is large ($V_1<2$) to a phase where it is very small (V_1

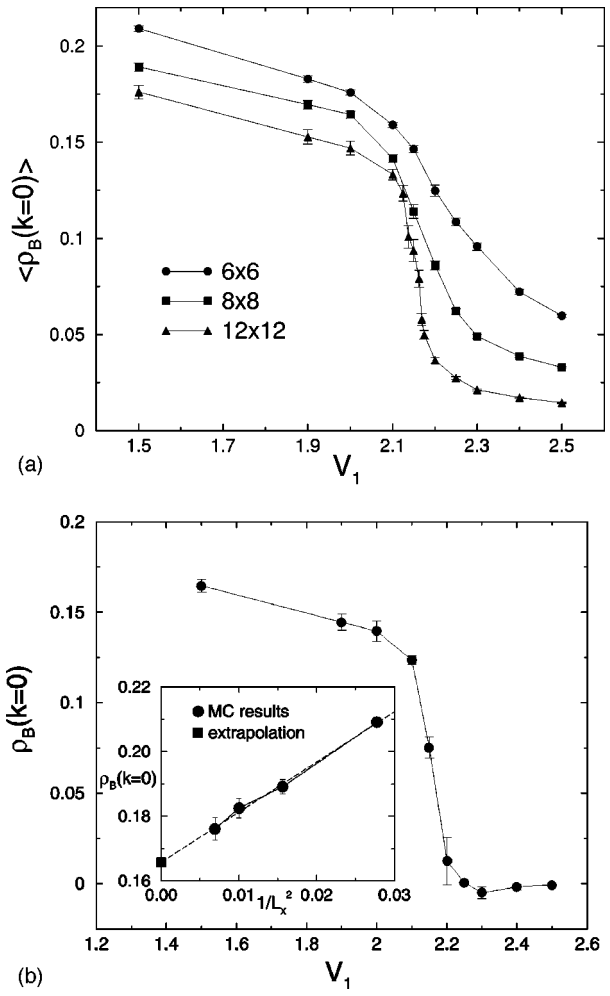

FIG. 11. (a) The filling fraction of the $k_x=0$ mode versus the interaction V_1 ($V_2=0$) for different sizes. The systems are half filled and $\beta=6$. (b) The filling fractions of Fig. 11(a) extrapolated to infinite systems. Inset: Filling fraction versus inverse system size for $V_1=1.5$.

>2). The inset of Fig. 11(b) shows that the extrapolation of $\rho_B(k_x=0)$ to the infinite system is linear in the inverse system size. The extrapolated values are shown in Fig. 11(b) exhibiting clearly the phase transition from non-zero to zero condensate density.[20] Figure 12 shows ρ_s versus V_1 as directly measured from the winding number. We see that the behavior is exactly the same as for the condensate fraction, $N(k_x=0)$, in Fig. 11. The transition of ρ_s to zero goes hand in hand with that of the condensate fraction. These results for ρ_s and the zero-mode filling fraction show that the transition from superfluid to (π,π)-solid is continuous when $V_2=0$.

The question of what happens when this system is doped away from $\rho=0.5$ is not simple for large V_1 and has been addressed elsewhere.[19]

So far we have discussed the two limits $(V_1=0,V_2\neq 0)$ and $(V_1\neq 0,V_2=0)$. To construct the phase diagram in the (V_1,V_2) plane we need to do simulations with both interactions nonzero. This was done in Ref. 12 for $V_1\leqslant 4.6,V_2\leqslant 3$ where it was found that within these values of the interactions there was no direct (π,π)-solid to $(\pi,0)$-solid transition although mean field calculations predict this to happen starting at $(V_1=4,V_2=2)$.[12] Here we extend the simulations

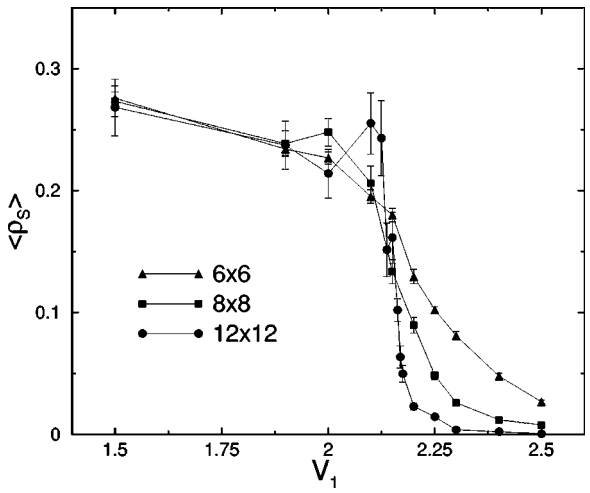

FIG. 12. The superfluid density versus the interaction V_1 ($V_2=0$) and for different sizes. The systems are half filled and $\beta=6$.

farther. Figure 13 shows ρ_s, $S(\pi,\pi)$, and $S(\pi,0)$ as a function of V_2 for $V_1=6$. We see that even at this large value of V_1 there is no direct solid-solid transition. In addition, the sharpness of the superfluid to $(\pi,0)$-solid transition suggests that it is first order while the relative smoothness of the superfluid to (π,π)-solid suggests that it is continuous. This is in agreement with Refs. 12 and 19. Preliminary results indicate that even at $V_1=8$ there still is no solid to solid transition. Apparently, the frustration caused by the competition between V_1 and V_2 prevents this and always results in a superfluid phase separating the two solid phases for any large but finite $V_{1,2}$.

One of our goals in searching the phase diagram is to explore the possibility of a normal state at zero temperature. This is a particularly interesting question since such states have been found experimentally in high-T_c superconductors. Explanations offered so far rely on the idea that the charge carriers in this normal state are the Cooper pairs, and thus bosonic. However, the models which have been examined are for soft core bosons at high densities. Our simulations for hard core bosons have not shown any candidates for such a

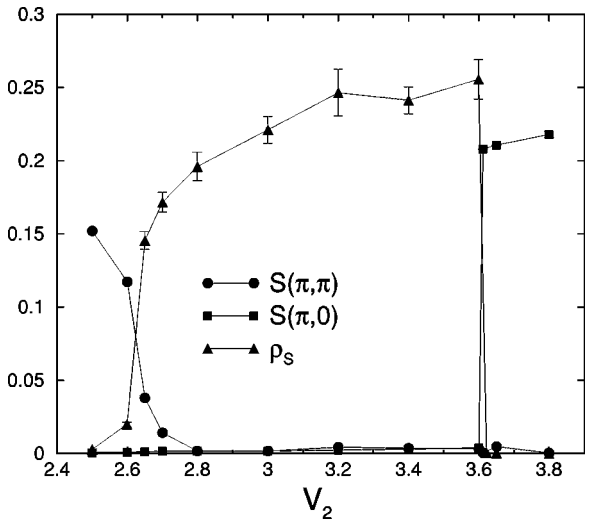

FIG. 13. $S(\pi,\pi)$,$S(\pi,0)$ and ρ_s versus V_2 for $V_1=6$. There is no solid-solid transition even at this large value of V_1.

normal state. All phases we found so far are clearly solid, superfluid or solid as shown, for example, in Fig. 13.

VI. CONCLUSION

We have detailed the construction and testing of a quantum Monte Carlo algorithm based on the exact duality transformation of the bosonic Hubbard model. In particular we showed that this formulation yields a particularly simple dual partition function in the very important case of hardcore bosons. We also showed how to measure various physical quantities. In particular, we showed how to measure the Green function, an important quantity, which is particularly difficult to obtain with other algorithms. To improve the statistics of this quantity we enhanced the efficiency of the algorithm by introducing a reweighting procedure.

We then used this algorithm to elaborate the structure of the various ground-state phases of the bosonic Hubbard model. In particular, we showed and interpreted the behavior of the Green function in the various superfluid, supersolid, and solid phases and calculated the filling fraction in the zero momentum mode. We found a filling fraction of about 33% at weak nn coupling, $V_1=1.5$. This value is consistent with the pure hardcore value of Ref. 21 (between 36% and 22%). However, the two results were obtained at different boson densities and at the moment it is not clear how our value depends on the density. This is in progress.

We confirmed that the order of the phase transition from the superfluid to the solid phases depends on the long-range order. At half filling, the SF-(π,π)-solid transition is second order while the SF-$(\pi,0)$-solid transition is first order.

The presence of a direct solid-solid transition from (π,π) to $(\pi,0)$ is still an open question although the indications are that it is not present at any finite value of $V_{1,2}$. Another important issue is the possibility of a normal conducting phase. Several different scenarios for the existence of normal conducting states in two dimensions have been offered but for softcore bosons. So far, our exploration of the phase diagram of this hardcore bosonic model have given no hints of the presence of such a state.

ACKNOWLEDGMENTS

We acknowledge very fruitful discussions with H. Rieger and R. T. Scalettar. G.G.B. thanks the Physics Department at U.C. Davis for its hospitality.

APPENDIX: DERIVATION OF THE DUAL PARTITION FUNCTION

We present in some detail the integration of the original fields to obtain the dual expression for Z. Then we show, using hardcore bosons as an example, how to simplify this expression by explicitly solving constraints appearing in it.

1. General partition function

To integrate out the bond variable Θ and the amplitude ρ in Eq. (29), we expand the exponentials of complex exponentials in Taylor series. This results in new integer variables $l_{r,\tau}$, $p^{(i)}_{r,\tau}$, and $q^{(i)}_{r,\tau}$. l arises from the expansion of the second exponential in Eq. (29), $p^{(i)}$ and $q^{(i)}$ from the i^{th} hopping term

$$
\begin{aligned}
Z=\sum\int\prod_{r,\tau}\Bigg\{ & \rho_{r,\tau}\frac{d\rho_{r,\tau}}{\pi}\tilde{\rho}_{r,\tau}\frac{d\tilde{\rho}_{r,\tau}}{\pi}d\Theta^1_{r,\tau}d\Theta^0_{r,\tau}d\tilde{\Theta}^0_{r,\tau}\\
&\times e^{(-\rho^2_{r,\tau}-\tilde{\rho}^2_{r,\tau})}e^{-\delta V(n_{r,\tau})}\\
&\times\frac{(\delta t)^{p^{(1)}_{r,\tau}+q^{(1)}_{r,\tau}}(\delta^2t^2/2!)^{p^{(2)}_{r,\tau}+q^{(2)}_{r,\tau}}\cdots}{n_{r,\tau}!l_{r,\tau}!p^{(1)}_{r,\tau}!q^{(1)}_{r,\tau}!p^{(2)}_{r,\tau}!q^{(2)}_{r,\tau}!\cdots}\\
&\times\tilde{\rho}^{[n_{r,\tau}+l_{r,\tau-1}+p^{(1)}_{r-1,\tau-1}+q^{(1)}_{r,\tau-1}+p^{(2)}_{r-2,\tau-1}+q^{(2)}_{r,\tau-1}+\cdots]}_{r,\tau}\\
&\times\rho^{[n_{r,\tau}+l_{r,\tau}+p^{(1)}_{r,\tau}+q^{(1)}_{r-1,\tau}+p^{(2)}_{r,\tau}+q^{(2)}_{r-2,\tau}+\cdots]}_{r,\tau}\\
&\times e^{-i\tilde{\Theta}^0_{r,\tau}[l_{r,\tau}+p^{(1)}_{r-1,\tau}+q^{(1)}_{r,\tau}+p^{(2)}_{r-2,\tau}+q^{(2)}_{r,\tau}+\cdots-J^0_{r,\tau}-N^0_r]}\\
&\times e^{-i\Theta^1_{r,\tau}[p^{(1)}_{r,\tau}-q^{(1)}_{r,\tau}+p^{(2)}_{r,\tau}+p^{(2)}_{r-1,\tau}-q^{(2)}_{r,\tau}-q^{(2)}_{r-1,\tau}+\cdots-J^1_{r,\tau}-N^1_{r,\tau}]}\\
&\times e^{-i\Theta^0_{r,\tau}[n_{r,\tau}-J^0_{r,\tau-1}-N^0_r]}\Bigg\},
\end{aligned}
\tag{A1}
$$

where the sum runs over all the discrete indices we have introduced: l, p, q, J, N, and n. Integrating over Θ^1, Θ^0, and $\tilde{\Theta}^0$ will give three constraints on the dual variables enforced by Kronecker deltas. The constraint coming from the integration over $\Theta^0_{r,\tau}$, enforces the condition

$$
J^0_{r,\tau-1}+N^0_r=n_{r,\tau}. \tag{A2}
$$

The total conserved current $J^\mu_{r,\tau}+N^\mu_{r,\tau}$ is then just the current of bosons crossing the lattice. Negative time currents are not allowed: Bosons cannot go backward in imaginary time.

Using the two remaining constraints, one can see that the power of $\tilde{\rho}_{r,\tau}$ is $2(J^0_{r,\tau-1}+N^0_r)$. The integration over $\tilde{\rho}$ then yields a $(J^0_{r,\tau}+N^0_r)!$ which compensates the $1/n_{r,\tau}!=1/(J^0_{r,\tau}+N^0_r)!$ already present in the expression.

The remaining ρ integrals are Gaussian and can be performed easily. This leads to the dual formulation of Z:

$$
\begin{aligned}
Z=\sum\prod_{r,\tau}\Bigg\{ & e^{-\delta V(J^0_{r,\tau}+N^0_{r,\tau})}\\
&\times\frac{(\delta t)^{(p^{(1)}_{r,\tau}+q^{(1)}_{r,\tau})}(\delta^2t^2/2!)^{(p^{(2)}_{r,\tau}+q^{(2)}_{r,\tau})}\cdots}{l_{r,\tau}!p^{(1)}_{r,\tau}!q^{(1)}_{r,\tau}!p^{(2)}_{r,\tau}!q^{(2)}_{r,\tau}!\cdots}\\
&\times\Gamma\Bigg(1+\frac{1}{2}[l_{r,\tau}+l_{r,\tau+1}+p^{(1)}_{r-1,\tau}+p^{(1)}_{r,\tau+1}+q^{(1)}_{r,\tau}\\
&+q^{(1)}_{r-1,\tau+1}+\cdots]\Bigg)\times\delta(l_{r,\tau}+p^{(1)}_{r-1,\tau}+q^{(1)}_{r,\tau}+p^{(2)}_{r-2,\tau}\\
&+q^{(2)}_{r,\tau}+\cdots-J^0_{r,\tau}-N^0_r)\,\delta(p^{(1)}_{r,\tau}-q^{(1)}_{r,\tau}+p^{(2)}_{r,\tau}+p^{(2)}_{r-1,\tau}\\
&-q^{(2)}_{r,\tau}-q^{(2)}_{r-1,\tau}+\cdots-J^1_{r,\tau}-N^1_\tau)\Bigg\},
\end{aligned}
\tag{A3}
$$

where the sum runs over all the remaining integer indices l, p, q, and the conserved current $J+N$.

It is impossible to construct an efficient Monte Carlo algorithm using this equation: There are many different fields, and many constraints. If one proposes a trial move, it will be rejected most of the time because it does not respect the conditions imposed by the δ's or the factorials.

Of course the role of the δ functions is to allow only the acceptable configurations and give them the correct weight. It is possible to simplify greatly this partition function by solving these constraints, i.e., by finding the allowed configurations of currents and the corresponding weights. We now show how to do this for the case of hardcore bosons.

2. Hardcore bosons

To impose the hard core limit, we require the number of particles not be greater than 1 on any site. This is achieved simply by imposing that $J^0_{r,\tau}+N^0_r=0,1$ and $|J^1_{r,\tau}+N^1_{r,\tau}|=0,1$ on all bonds. It is also understood that the currents must always be conserved.

Now we need to find the Boltzmann weights of the allowed configurations. To do this we calculate the weights of representative boson (i.e., current) configurations. The contributions of the interaction and chemical potential are very simple to include. We have an $\exp(\delta\mu)$ factor for each nonzero time-current element, and an $\exp(-\delta V_1)$ for each pair of near neighbor time currents.

For example, consider configuration (a) in Fig. 14 where the time current, $J^0_{r,\tau}+N^0_r$, is 1 along the directed path shown and zero everywhere else. This configuration satisfies all the constraints, and is uniquely specified by having all integer fields equal to zero except for the l field along the directed path where it is equal to 1. This is shown in the figure. So the Boltzmann weight of this configuration is simply

$$\prod_\tau e^{\delta\mu}\Gamma(2)=(e^{\delta\mu})^{L_\tau}=e^{\beta\mu}, \tag{A4}$$

which agrees with intuitive expectations.

Now consider path (b) in Fig. 14. Clearly, this is an allowed configuration and as before we determine, by explicit calculation, the values of the integer fields that give it. These are shown in the figure. The Boltzmann weight of this configuration is therefore:

$$(e^{\delta\mu})^{L_\tau}(\delta t)^2[\Gamma(2)]^{L_\tau}=e^{\beta\mu}(\delta t)^2. \tag{A5}$$

The physical picture that emerges is simple: We always have the usual chemical potential factor and when the current line jumps from one site to another, we have a contribution of the hopping term. The l are nonzero where there are time currents, the p where there is a jump to the right, and the q where there is a jump to the left. As a third example, to fix ideas, consider path (c) in Fig. 14. It has one double jump and two single ones. Therefore, we now have one non-zero $p^{(2)}$, corresponding to the double jump to the right, and two $q^{(1)}$ for the two single jumps to the left. The weight of this configuration is

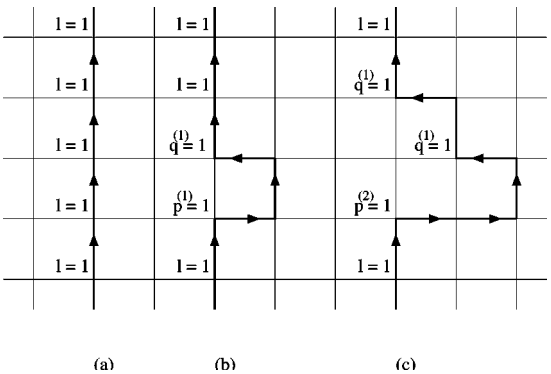

FIG. 14. Different configurations of the conserved current. (a) Without jumps, (b) with two single jumps, and (c) with one double jump and two single ones. The nonzero values of the integer dual variables are indicated.

$$\frac{\delta^2 t^2}{2!}(\delta t)^2 e^{\beta\mu}. \tag{A6}$$

Thus, in the hardcore limit, the partition function simplifies drastically. Only one field survives: The conserved hard core current. The weight of a configuration can be easily calculated as follows:

$$Z=\sum_{\{J,N\}}{}' \mathcal{P}(N,J)=\sum_{\{J,N\}}{}' \prod_L \left\{\left[\frac{(\delta t)^L}{L!}\right]^{N_l}\right\} e^{-\delta V_1 N_{V_1}} e^{\beta\mu N_B}, \tag{A7}$$

where N_L is the number of jumps of length L, N_{V_1} is the number of near-neighbor time current on the lattice, N_b is simply the number of bosons, and $\mathcal{P}$ is the Boltzmann weight. As mentioned in the main body of the paper, this partition function has systematic Trotter error of order δ. If one wants to construct an algorithm accurate to order δ^2, one would have to keep track of all the second order terms all along the development of the kinetic term.

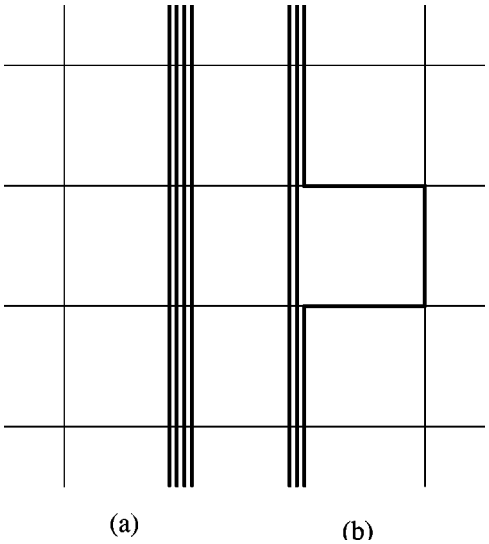

FIG. 15. Configuration with softcore bosons. (a) Four bosons at the same site, (b) three bosons at the same site and one of them hopping to a neighboring site.

One can generalize this approach to other kinds of systems. For example if we look at the soft core configurations shown in Fig. 15(a), four bosons cross the lattice on the same site without hopping. The only nonzero field is $l_{r',\tau}$ and we get the weight

$$\left(\frac{1}{4!}\Gamma(5)e^{4\delta\mu-6\delta V_0}\right)^{L_\tau}=e^{\beta(4\mu-6V_0)}, \tag{A8}$$

which is the expected result. Configuration (b) of Fig. 15 with three bosons on the same site and one of them hopping to a neighboring site contributes

$$3e^{3\beta\mu}e^{-\delta V_0(3L_\tau-2)}e^{-2\delta V_1}(\delta t)^2. \tag{A9}$$

The prefactor 3 can be interpreted physically: Each boson can make this jump with equal probability and the sum must be taken (Fig. 15).

[1] H. A. Kramers and G. H. Wannier, Phys. Rev. **60**, 252 (1941).

[2] See, for example, the review articles: J. B. Kogut, Rev. Mod. Phys. **51**, 659 (1979); R. Savit, *ibid.* **52**, 453 (1980), and references therin.

[3] G. G. Batrouni, Nucl. Phys. B **208**, 467 (1982); G. G. Batrouni and M. B. Halpern, Phys. Rev. D **30**, 1775 (1984).

[4] C. P. Burgess and F. Quevedo, Nucl. Phys. B **421**, 373 (1994); C. P. Burgess, C. A. Lütken, and F. Quevedo, Phys. Lett. B **336**, 18 (1994).

[5] M.-C. Cha *et al.* Phys. Rev. B **44**, 6883 (1991).

[6] J. Villain, J. Phys. (France) **36**, 581 (1975).

[7] A. van Otterlo and K-H. Wagenblast, Phys. Rev. Lett. **72**, 3598 (1994).

[8] L. Amico, G. Falci, R. Fazio, and G. Giaquinta, Phys. Rev. B **55**, 1100 (1997).

[9] I. Herbut, Phys. Rev. B **57**, 13 729 (1998).

[10] J. E. Hirsch, R. L. Sugar, D. J. Scalapino, and R. Blankenbecler, Phys. Rev. B **26**, 5033 (1982).

[11] G. G. Batrouni, R. T. Scalettar, and G. T. Zimanyi, Phys. Rev. Lett. **65**, 1765 (1990); **66**, 3144 (1991); P. Niyaz, R. T. Scalettar, C. Y. Fong, and G. G. Batrouni, Phys. Rev. B **44**, 7143 (1991); **50**, 362 (1994); G. G. Batrouni and R. T. Scalettar, *ibid.* **46**, 9051 (1992); G.G. Batrouni, B. Larson, R. T. Scalettar, J. Tobochnik, and J. Wang, *ibid.* **48**, 9628 (1993).

[12] G. G. Batrouni, R. T. Scalettar, G. T. Zimanyi, and A. P. Kampf, Phys. Rev. Lett. **74**, 2527 (1995); R. T. Scalettar, G. G. Batrouni, A. P. Kampf, and G. T. Zimanyi, Phys. Rev. B **51**, 8467 (1995).

[13] H. G. Evertz, G. Lana, and M. Marcu, Phys. Rev. Lett. **70**, 875 (1993); U.-J. Wiese and H.-P. Ying, Phys. Lett. A **168**, 143 (1992); Z. Phys. B: Condens. Matter **93**, 147 (1994); N. Kawashima, J. E. Gubernatis, and H. G. Evertz, Phys. Rev. B **50**, 136 (1994); N. Kawashima and J. E. Gubernatis, Phys. Rev. Lett. **73**, 1295 (1994).

[14] B. B. Beard and U.-J. Wiese, Phys. Rev. Lett. **77**, 5130 (1996).

[15] N. V. Prokof'ev *et al.*, Phys. Lett. A **238**, 253 (1998); Sov. Phys. JETP **87**, 310 (1998).

[16] A. Sandvik, Phys. Rev. B **59**, R14 157 (1999).

[17] J. W. Negele and H. Orland, *Quantum Many-Particle Systems* (Perseus Books, Reading, Massachusetts, 1998).

[18] The symmetry breaking is, of course, not spatial. It is the $U(1)$ symmetry of the Hamiltonian which is broken when the system becomes superfluid.

[19] G. G. Batrouni and R. T. Scalettar, cond-mat/9909198.

[20] It is important to keep in mind that these extrapolated values still include some Trotter error due to the discretization of imaginary time. Also, although the temperature is low ($\beta=6$) it is not zero, this will introduce some corrections too.

[21] P. Whitlock, G. V. Chester, and M. Kalos, Phys. Rev. B **38**, 2418 (1988).